Molecular Therapy
Oncolytics
Original Article

Oncolytic herpes simplex virus armed with a bacterial GBP1 degrader improves antitumor activity

Jun Xie,[1,2] Shaowei Wang,[1,2] Yunhong Zhong,[1,2] Ming Gao,[1,2] Xuezhang Tian,[1,2] Liting Zhang,[1,2] Dongli Pan,[3,4] Qingsong Qin,[5] Bing Wu,[2] Ke Lan,[2,6] Zhi-Jun Sun,[7] and Junjie Zhang[1,2]

[1]The State Key Laboratory Breeding Base of Basic Science of Stomatology & Key Laboratory of Oral Biomedicine Ministry of Education, School & Hospital of Stomatology, State Key Laboratory of Virology, Medical Research Institute, Wuhan University, Wuhan 430071, China; [2]Frontier Science Center for Immunology and Metabolism, Wuhan University, Wuhan 430071, China; [3]State Key Laboratory for Diagnosis and Treatment of Infectious Diseases, the First Affiliated Hospital, Zhejiang University School of Medicine, Hangzhou 310003, China; [4]Department of Medical Microbiology and Parasitology, Zhejiang University School of Medicine, Hangzhou 310058, China; [5]Laboratory of Human Virology and Oncology, Shantou University Medical College, Shantou, Guangdong 515041, China; [6]State Key Laboratory of Virology, School of Life Sciences, Wuhan University, Wuhan 430072, China; [7]The State Key Laboratory Breeding Base of Basic Science of Stomatology (Hubei-MOST) & Key Laboratory of Oral Biomedicine Ministry of Education, School & Hospital of Stomatology, Wuhan University, Wuhan 430079, China

Oncolytic viruses (OVs) encoding various transgenes are being evaluated for cancer immunotherapy. Diverse factors such as cytokines, immune checkpoint inhibitors, tumor-associated antigens, and T cell engagers have been exploited as transgenes. These modifications are primarily aimed to reverse the immunosuppressive tumor microenvironment. By contrast, antiviral restriction factors that inhibit the replication of OVs and result in suboptimal oncolytic activity have received far less attention. Here, we report that guanylate-binding protein 1 (GBP1) is potently induced during HSV-1 infection and restricts HSV-1 replication. Mechanistically, GBP1 remodels cytoskeletal organization to impede nuclear entry of HSV-1 genome. Previous studies have established that IpaH9.8, a bacterial E3 ubiquitin ligase, targets GBPs for proteasomal degradation. We therefore engineered an oncolytic HSV-1 to express IpaH9.8 and found that the modified OV effectively antagonized GBP1, replicated to a higher titer *in vitro* and showed superior antitumor activity *in vivo*. Our study features a strategy for improving the replication of OVs via targeting a restriction factor and achieving promising therapeutic efficacy.

INTRODUCTION

Cancer immunotherapy exemplified by immune checkpoint blockade (ICI) has revolutionized cancer treatment.[1] Despite the success of ICIs, a majority of patients do not respond or fail to achieve durable clinical benefit. Resistance to ICIs has been linked with the lack of tumor-associated antigens (TAAs), poor antigen presentation, absence of tumor-infiltrating immune cells, and the immunosuppressive tumor microenvironment that blunts the killing activity of effector T cells and adoptively transferred T cells.[2,3] To tackle these problems, various combination strategies are being actively pursued to overcome the primary and acquired resistance associated with ICI treatment. Among them, oncolytic viruses (OVs) are emerging as a versatile platform to unleash the full potential of cancer immunotherapy.[4] OVs are wild-type (WT) or genetically engineered viruses that selectively replicate in tumor cells. The replication of OVs results in highly immunogenic cancer cell death, with the release of TAAs, pathogen-associated molecular patterns, and damage-associated molecular patterns, which together promote the activation of antigen-presenting cells (APCs) and the subsequent priming and activation of antitumor cytotoxic T cells.[4] In addition, the release of cytokines and chemokines in the tumor microenvironment upon OV administration promotes the infiltration of immune cells, including dendritic cells (DCs) and $CD8^+$ T cells.[4] Furthermore, the replication of OVs overturns the immunosuppressive tumor microenvironment to reinvigorate exhausted T cells.[4] These advantages have put OVs in a good position to be administered alone, or in combination with other cancer immunotherapies, such as ICIs for cancer treatment.[4,5] The clinical effectiveness of OVs has led to Food and Drug Administration (FDA) approval of talimogene laherparepvec (T-VEC), a genetically modified oncolytic virus based on HSV-1, for the treatment of advanced melanoma.[6] Despite the clinical benefits of OVs, with the monotherapy efficacy of T-VEC being around 16% in melanoma patients,[7,8] there is still great room for improvement.

Recently, considerable effort has been devoted to the development of genetically modified OVs encoding various transgenes to improve

Received 13 January 2023; accepted 24 April 2023;
https://doi.org/10.1016/j.omto.2023.04.006.

Correspondence: Zhi-Jun Sun, The State Key Laboratory Breeding Base of Basic Science of Stomatology (Hubei-MOST) & Key Laboratory of Oral Biomedicine Ministry of Education, School & Hospital of Stomatology, Wuhan University, Wuhan 430079, China.
E-mail: sunzj@whu.edu.cn
Correspondence: Junjie Zhang, The State Key Laboratory Breeding Base of Basic Science of Stomatology & Key Laboratory of Oral Biomedicine Ministry of Education, School & Hospital of Stomatology, State Key Laboratory of Virology, Medical Research Institute, Wuhan University, Wuhan 430071, China.
E-mail: junjiezhang@whu.edu.cn

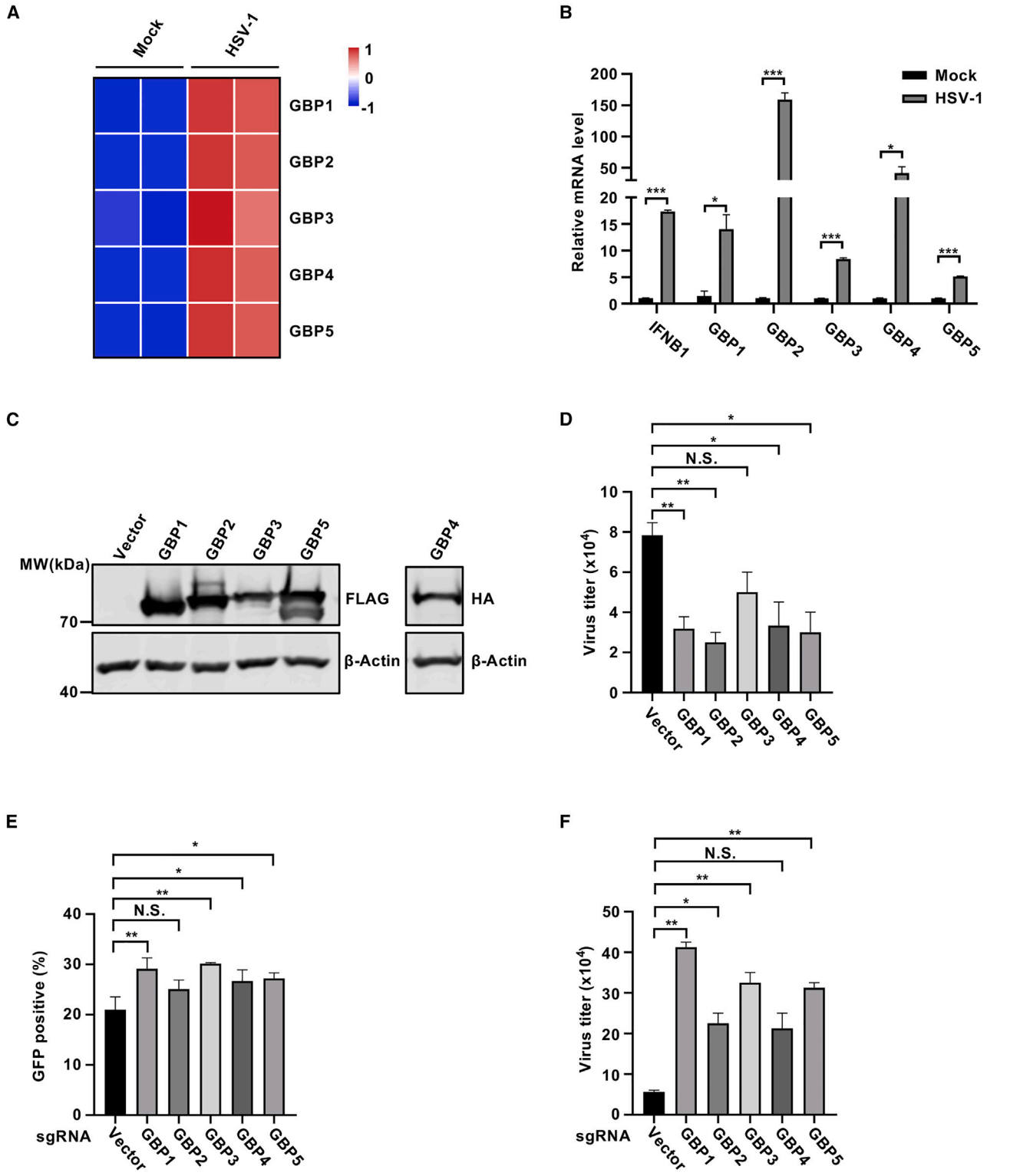

Figure 1. GBPs are induced by HSV-1 and restrict HSV-1 replication

THP-1 cells were infected with HSV-1 (MOI = 5) and RNA was extracted at 8 h post-infection and subjected to RNA sequencing analysis. The heatmap summarizes the relative expression of GBPs (A). The expression of GBPs and IFNB1 was determined by RT-qPCR at 8 h post-infection (B). HEK293T cells were transfected with vector or

(legend continued on next page)

therapeutic efficacy. For example, granulocyte-macrophage colony-stimulating factor (GM-CSF), carried in T-VEC, functions as an immune adjuvant to augment the recruitment and activation of APCs.[9] Other than cytokines, TAAs, ICIs, and T cell engagers have also been exploited as transgenes to improve OV therapies. These genetic modifications show various positive effects in preclinical animal models.[4] However, these efforts mainly focus on modulating host immune responses and/or the tumor microenvironment. The improvement on the replication capacity of OVs per se has received far less attention. Most OVs are genetically modified to attenuate viral pathogenesis, resulting in impaired viral replication. For example, ICP34.5 has been deleted in T-VEC to reduce neurovirulence.[10] However, ICP34.5 deficiency leads to enhanced antiviral innate immunity and autophagy, which significantly impairs viral replication.[11,12] In another study, interferon signaling activation has been found to play a key role in restricting oncolytic measles virus replication in glioblastoma treatment.[13] Therefore, elucidating critical restriction factors in OV therapies and developing OVs that can counteract these restriction factors would greatly advance the replication of OVs and improve OV therapeutic efficacy.

Interferon (IFN)-induced guanylate-binding proteins (GBPs), belonging to a large IFN-induced GTPase family, play a critical role in cell-autonomous defense against bacterial infections.[14,15] Upon bacterial invasion, GBP1, the founding member of the GBP family, compromises bacteria-containing vesicles or directly targets free bacteria. Moreover, GBPs are critical to the activation of inflammasome, which coordinates antimicrobial inflammatory responses for bacterial elimination.[14,15] To antagonize the restrictive activity of GBPs, a Shigella-encoded effector protein IpaH9.8 targets GBPs for proteasomal degradation to facilitate bacterial replication.[16] By contrast, the role of GBPs in virus infection is less studied despite that GBPs are highly induced by viral infection.[15] Notably, GBP1 has been reported to remodel actin cytoskeleton to inhibit KSHV infection.[17] It remains uncharacterized whether and how GBPs inhibit oncolytic herpes simplex virus replication, and whether GBPs can be targeted to improve OV therapies.

In this study, we report that GBP1 is highly induced by HSV-1 and potently inhibits viral replication. Both the prenylation and ATPase activities of GBP1 are required to restrict HSV-1 infection. Mechanistically, GBP1 remodels cytoskeletal organization of the infected cells to hinder the delivery of HSV-1 genome into the nucleus. Based on these findings, we have engineered an oncolytic HSV-1 that recombinantly expresses IpaH9.8 to augment the replication of the oncolytic virus. Compared with the prototype OV, the modified OV armed with IpaH9.8 effectively antagonizes GBP1 and replicates to a higher titer *in vitro* and demonstrates stronger antitumor activity *in vivo*. Our study features a strategy via targeting a restriction factor to promote the replication of OVs and achieve enhanced therapeutic efficacy.

RESULTS

GBPs are induced by HSV-1 and restrict HSV-1 replication

Previously, we performed RNA sequencing to profile the transcriptional changes of human monocyte THP-1 cells infected with HSV-1.[18] THP-1 cells are immune cells that are highly responsive to virus infection and are commonly used to study HSV-1-induced innate immune responses.[18,19] Notably, the GBP family members including GBP1-5 were significantly induced by HSV-1 (Figure 1A). Real-time PCR analysis confirmed that HSV-1 infection potently stimulated the expression of GBP1-5 (Figure 1B). Consistent with previous reports, HSV-1 infection induced antiviral innate immune responses, as indicated by the potent induction of *IFNB1* (Figure 1B).[19] Considering the role of GBPs in antimicrobial defense, we hypothesized that GBPs may restrict HSV-1 replication. To test this hypothesis, we first transiently expressed GBP1-5 in HEK293T cells and then performed HSV-1 infection (Figure 1C). HEK293T cells were used for transient transfection due to their high transfection efficiency.[20,21] We found that except for GBP3, the other GBPs were able to suppress the production of progeny virions (Figure 1D). Our data suggest that the expression of GBP3 alone is insufficient to restrict HSV-1 replication. To corroborate these results, we ablated the expression of GBP1-5 using CRISPR-Cas9 technology in THP-1 cells and then infected the knockout cells with GFP-HSV-1. Except for GBP2 and GBP4, deficiency of the other GBPs enabled enhanced replication of HSV-1, as indicated by the enhanced GFP expression and the increased production of progeny virions compared with WT cells (Figures 1E and 1F). These data suggest that HSV-1-induced GBP2 and GBP4 are relatively weak at restricting viral replication (Figures 1E and 1F), although they are sufficient to suppress HSV-1 replication when overexpressed in HEK293T cells. Together, these data indicate that GBPs are induced by HSV-1 and restrict HSV-1 replication.

GBP1 suppresses HSV-1 replication

Based on our observations, we found that GBP1 was among one of the most potent GBPs in terms of restricting HSV-1 replication, and knockout of GBP1 most potently promoted HSV-1 replication (Figure 1F). Moreover, GBP1 is the founding member of the GBP family and plays critical roles in host defense against bacteria and viruses.[15] We therefore focused on GBP1 for further studies. HT1080 cells were chosen for most of the antiviral and mechanistic investigations, as they are a human epithelial cell line that is more physiologically relevant to HSV-1 infection.[22,23] We first stably expressed GBP1 in HT1080 (Figure 2A) and found that GBP1 expression potently suppressed the replication of GFP-HSV-1 (Figure 2B). Plaque assays confirmed that GBP1 expression reduced the production of HSV-1 progeny virions (Figure 2C). Furthermore, HSV-1 gene transcription and viral protein expression were diminished in GBP1-expressing

FLAG-GBP1-5. At 24 h post-transfection, the cells were infected with HSV-1 (MOI = 0.01). Whole-cell lysates were analyzed by immunoblotting at 36 h post-infection (C). Viral titer was determined by plaque assay at 36 h post-infection (D). THP-1 cells were transduced with control sgRNA or sgRNA targeting GBP1-5, and the stable cells were infected with GFP-HSV-1 (MOI = 0.01) at 48 h post-transduction. GFP-positive cell percentage was determined at 24 h post-infection (E). Viral titer in the culture medium was determined by plaque assay at 24 h post-infection (F). Data are presented as means ± SEM, and statistical analyses were performed using a two-tailed unpaired Student's t test. Data are representative of three independent experiments. *$p < 0.05$; **$p < 0.01$; ***$p < 0.005$; N.S., not significant.

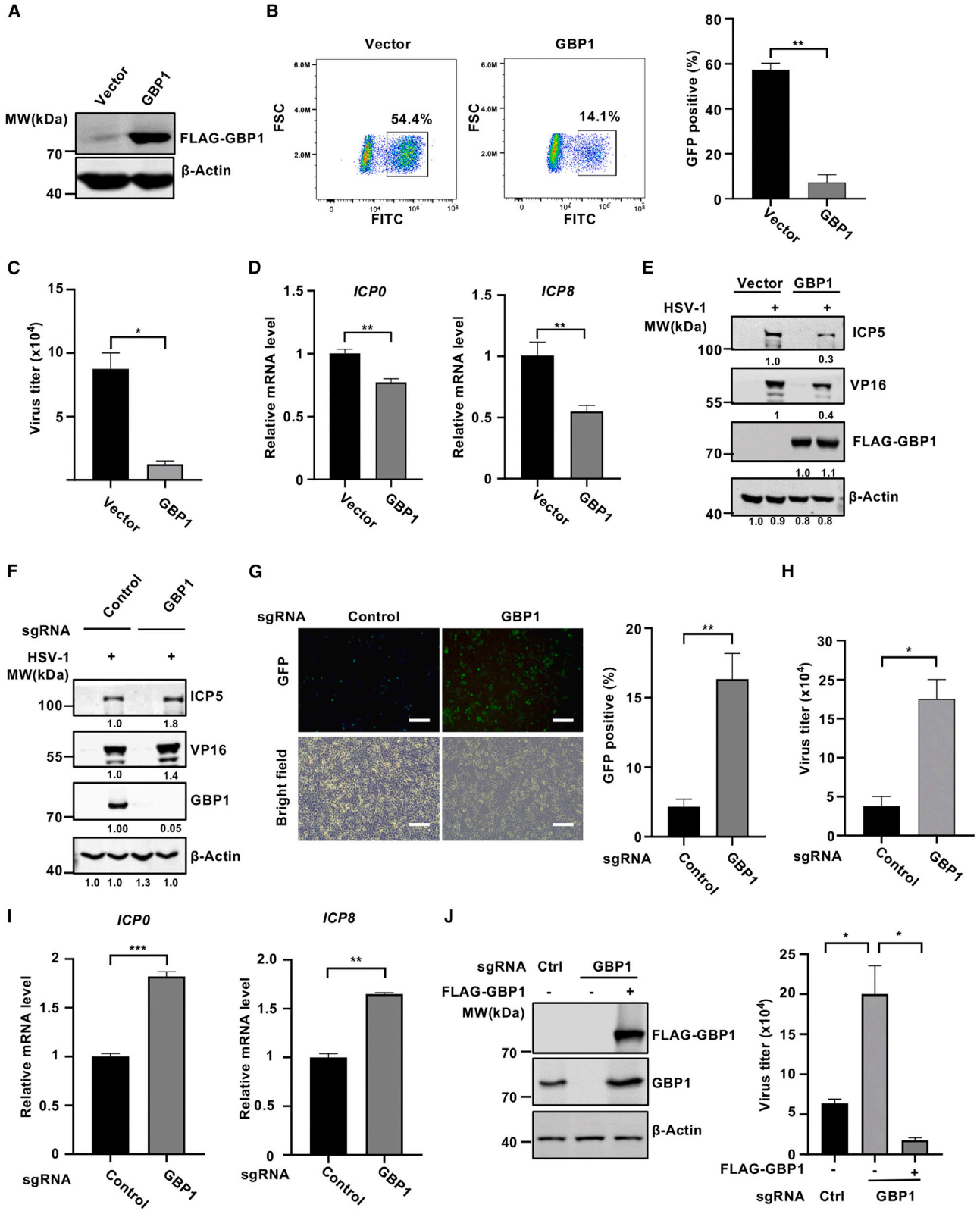

(legend on next page)

cells (Figures 2D and 2E). These data indicate that GBP1 suppresses HSV-1 replication. Next, we knocked out *GBP1* in HT1080 cells with CRISPR-Cas9 technology. GBP1 was induced by HSV-1 in control cells, while the expression of GBP1 could not be detected in the knockout cells (Figure 2F). Moreover, expression of viral proteins VP16 and ICP5 were increased in GBP1 knockout cells (Figure 2F). Consistently, HSV-1 replication was increased in GBP1-deficient cells, as indicated by the enhanced GFP fluorescence and increased viral titer (Figures 2G and 2H). Furthermore, GBP1 deficiency elevated HSV-1 gene expression (Figure 2I). Finally, we re-expressed GBP1 in GBP1-deficient cells and found that GBP1 reconstitution effectively suppressed HSV-1 replication (Figure 2J). Together, these data indicate that GBP1 restricts HSV-1 replication.

GBP1 blocks HSV-1 genome nuclear translocation

Next, we sought to investigate how GBP1 restricts HSV-1 replication. First, we infected control HT1080 or HT1080 stably expressing GBP1 with HSV-1 and quantified viral gene expression at different time points. Notably, GBP1 effectively blunted the expression of *ICP0* and *UL23* as early as 2 h post-infection (Figure 3A), suggesting that GBP1 functions as a restriction factor at an early stage of infection. Then we examined HSV-1 entry into host cells and found that GBP1 did not affect the entry step (Figure 3B). Next, we fractionated the cytoplasmic and nuclear compartments of the infected cells and quantified the viral genome in the nucleus. Our results indicate that GBP1 expression inhibited the nuclear entry of HSV-1 genome (Figure 3C). Consistently, knockout of GBP1 enhanced nuclear entry of HSV-1 genome (Figure 3D). These data suggest that GBP1 blocks HSV-1 genome nuclear translocation.

To confirm these results, we performed immunofluorescence staining to detect ICP5, the major capsid protein of HSV-1, to monitor the localization of viral capsid after *de novo* infection. U2OS cells were chosen for immunofluorescence staining since they have a distinct cell morphology and are widely used for immunostaining studies.[24] In control cells, ICP5 mainly accumulated in the vicinity of the nucleus, indicating the efficient nuclear trafficking of viral capsid. By contrast, ICP5 displayed an apparent cytoplasmic distribution in GBP1-expressing cells (Figures 3E and 3F). These results indicate that GBP1 hampers viral capsid trafficking. Then we labeled HSV-1 genome with 5-ethynyl-2′-deoxycytidine (EdC) and utilized click chemistry to monitor the localization of the incoming viral genome. Notably, HSV-1 genome effectively translocated into the nucleus in control cells, whereas nuclear localized viral genome was dramatically reduced in GBP1-expressing cells (Figures 3G and 3H). Consistently, knockout of GBP1 promoted nuclear trafficking of the HSV-1 genome (Figure 3I). These data indicate that GBP1 blocks HSV-1 genome nuclear translocation.

The GTPase activity and prenylation of GBP1 are required to restrict HSV-1 infection

To further dissect the role of GPB1 in HSV-1 infection, we generated R48A and S52N mutants, which abrogate the GTPase activity of GBP1, as well as a ΔCAAX mutant that abrogates the prenylation and membrane association activities of GBP1.[25,26] We stably introduced GBP1 or these mutants into HT1080 cells by lentiviral transduction. Consistently, WT GBP1 suppressed the replication of HSV-1, as indicated by reduced GFP expression and viral titer, diminished nuclear translocation of viral genome, and decreased viral gene transcription (Figures 4B–4E). By contrast, the R48A, S52N, and ΔCAAX mutants lost the ability to restrict HSV-1 infection (Figures 4B–4E). ICP5 immunofluorescence staining verified that HSV-1 capsid trafficking was not altered in the presence of these mutants (Figure 4F). EdC labeling of HSV-1 genome coupled with click chemistry further confirmed that these mutants were not able to restrict nuclear translocation of HSV-1 genome (Figure 4G). Together, these data indicate that the GTPase activity and prenylation of GBP1 are required to restrict HSV-1 infection.

GBP1 disturbs actin cytoskeleton to hinder nuclear translocation of HSV-1 genome

GBP1 remodels the host actin cytoskeleton, whereas HSV-1 hijacks the host cytoskeleton for capsid trafficking.[27–29] Therefore, we hypothesize that GBP1 disturbs actin cytoskeleton to hinder HSV-1 capsid trafficking. To test this hypothesis, we first treated HSV-1-infected cells with a widely used actin cytoskeleton polymerization inhibitor, cytochalasin D (CytoD), and found that CytoD treatment effectively disrupted cytoskeletal organization (Figure 5A) and impeded the nuclear translocation of the HSV-1 genome as expected (Figures 5B and 5C). Importantly, GBP1 expression rearranged the cytoskeleton and blocked HSV-1 genome nuclear trafficking akin to the antiviral effect of CytoD (Figures 5A–5C). Moreover, GBP1 plus CytoD showed no additive effect in reducing nuclear localization of the HSV-1 genome (Figure 5C). These data suggest that GBP1

Figure 2. GBP1 suppresses HSV-1 replication

(A) HT1080 cells were infected with control (Vector) lentivirus or that containing FLAG-GBP1 to generate stable cells. Whole-cell lysates were analyzed by immunoblotting at 48 h post-transduction. (B) HT1080 stable cells as described in (A) were infected with GFP-HSV-1 (MOI = 0.01). The GFP-positive cell percentage was determined at 36 h post-infection. Viral titer in the culture medium was determined by plaque assay at 36 h post-infection (C). HT1080 stable cells as described in (A) were infected with HSV-1 (MOI = 5). The expression of the indicated genes was determined by RT-qPCR at 6 h post-infection (D). Whole-cell lysates in (B) were analyzed by immunoblotting at 36 h post-infection (E). HT1080 was transduced with control sgRNA or sgRNA targeting GBP1 to generate stable cells, and the stable cells were infected with GFP-HSV-1 (MOI = 0.01). Whole-cell lysates were analyzed by immunoblotting at 36 h post-infection (F). GFP expression was imaged and GFP-positive cell percentage was quantified by flow cytometry at 36 h post-infection (G). Scale bars, 100 μm. Viral titer in the culture medium was determined by plaque assay at 36 h post-infection (H). The expression of the viral genes was determined by RT-qPCR at 6 h post-infection (MOI = 5) (I). (J) HT1080 GBP1 knockout cells were stably reconstituted with control vector or GBP1. The stable cells were infected with HSV-1 (MOI = 0.01). Whole-cell lysates were analyzed by immunoblotting, and viral titer was determined by plaque assay at 36 h post-infection. Data are presented as means ± SEM, and statistical analyses were performed using a two-tailed unpaired Student's t test. Data are representative of three independent experiments. *$p < 0.05$; **$p < 0.01$; ***$p < 0.005$; N.S., not significant.

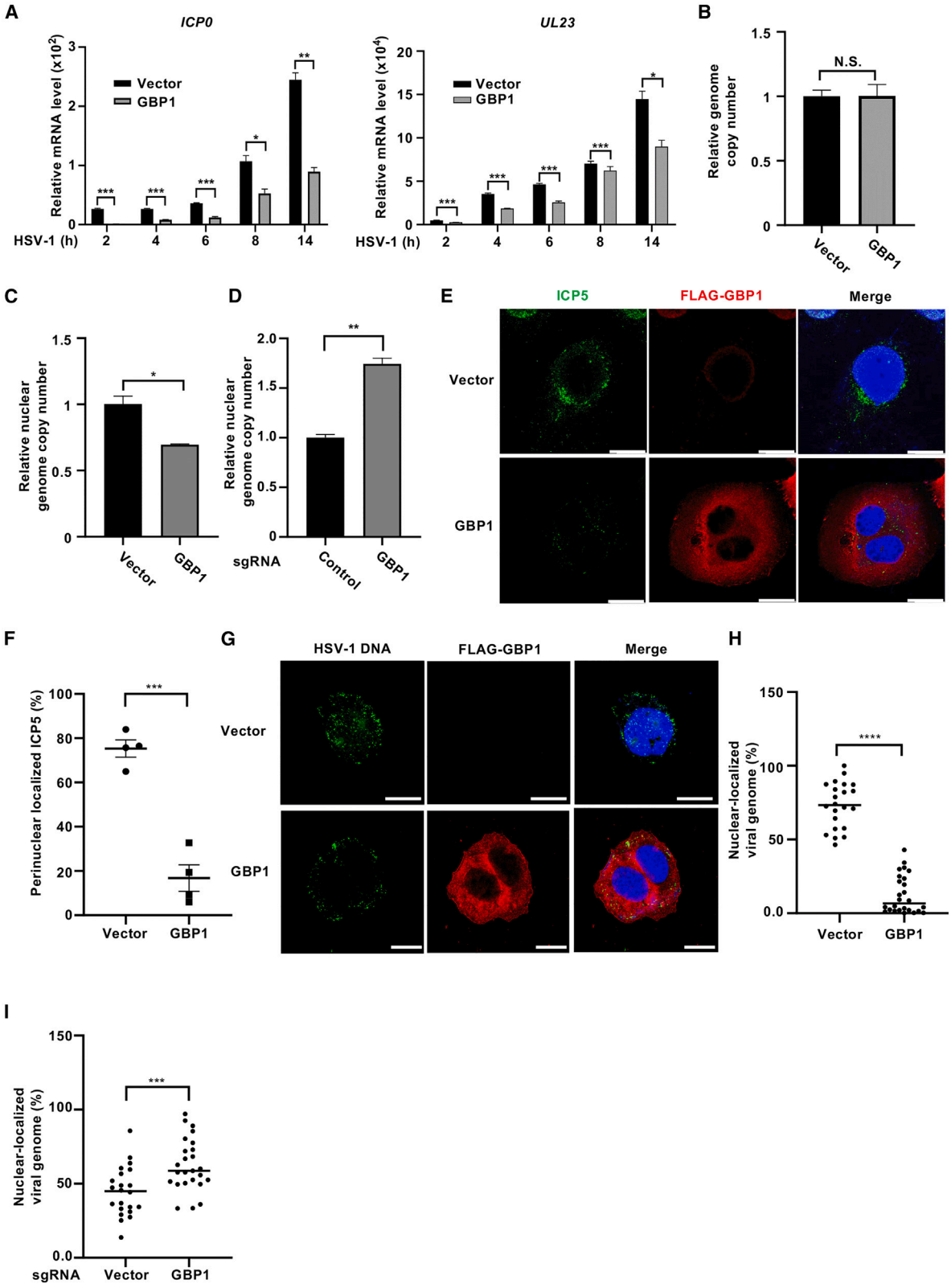

(legend on next page)

disturbs the cytoskeletal organization of infected cells to block nuclear trafficking of the HSV-1 genome.

Oncolytic HSV-1 armed with IpaH9.8 effectively antagonizes GBP1 to promote viral replication

Previous studies have established that Shigella-encoded effector protein IpaH9.8 specifically degrades GBPs to dampen host antimicrobial responses.[16,30] We reasoned that IpaH9.8 could be employed to disarm GBP1 for improving the replication of oncolytic HSV-1. We first tested the role of IpaH9.8 in HSV-1 infection. As expected, GBP1 expression in HEK293T cells suppressed HSV-1 replication, whereas the expression of IpaH9.8 negated the antiviral effect of GBP1 (Figures 6A and 6B). Furthermore, stable expression of IpaH9.8 in HT1080 fibroblasts abrogated the anti-HSV-1 activity of GBP1 (Figures 6C and 6D), indicating that IpaH9.8 functionally antagonizes GBP1 to promote HSV-1 replication. Building on these results, we engineered an oncolytic HSV-1 deficient in ICP34.5 and ICP47 (HSV-1 Δ34.5/Δ47; hereinafter referred to as oHSV) to express IpaH9.8 (HSV-1 Δ34.5/Δ47-IpaH9.8; hereinafter referred to as oHSV-IpaH9.8) (Figure 6E). We successfully detected the transcription of IpaH9.8 following oHSV-IpaH9.8 infection (Figure 6F). Compared with oHSV, oHSV-IpaH9.8 infection led to reduced GBP1 expression and enhanced viral late gene ICP5 expression (Figure 6G). Plaque assays confirmed that IpaH9.8 expression enhanced progeny infectious virion production in control cells, and the enhancing effect was more dramatic when these OVs were amplified in GBP1-expressing cells (Figure 6H). These data indicate that oncolytic HSV-1 armed with IpaH9.8 effectively antagonizes GBP1 to promote viral replication.

Oncolytic HSV-1 armed with IpaH9.8 demonstrates stronger antitumor activity

To evaluate the pathogenesis of the modified OVs, we intraperitoneally infected C57BL/6J mice with WT HSV-1, HSV-1 Δ34.5/Δ47 (oHSV) or HSV-1 Δ34.5/Δ47-IpaH9.8 (oHSV-IpaH9.8). Our results indicate that oHSV and oHSV-IpaH9.8 exhibited reduced pathogenesis compared with WT HSV-1, since they did not replicate in the mouse brain or induce inflammation like WT HSV-1 (Figure S1). Next, we sought to investigate whether oncolytic HSV-1 armed with IpaH9.8 has stronger oncolytic activity with a widely used MC38 syngeneic colorectal tumor model (Figure 7A). oHSV treatment slowed the growth of MC38 tumors as expected, but oHSV-IpaH9.8 administration showed stronger antitumor activity compared with oHSV (Figure 7B). oHSV treatment promoted the infiltration of $CD4^+$ and $CD8^+$ T cells, but the tumor infiltration of $CD4^+$ and $CD8^+$ T cells was further enhanced by oHSV-IpaH9.8, indicating that oHSV-IpaH9.8 stimulates stronger antitumor immune responses to suppress tumor growth (Figures S2, 7C, and 7D). Regarding the exhaustion status of $CD8^+$ T cells, both oHSV and oHSV-IpaH9.8 reduced the severely exhausted $CD8^+$ T cell population (Figure 7E). Next, we found that the percentage of $CD4^+$ and $CD8^+$ T cells in spleens was increased following the administration of oHSV and oHSV-IpaH9.8 (Figures 7F and 7G). We stimulated the splenocytes with phorbol 12-myristate 13-acetate (PMA) and ionomycin, and found that the production of interferon gamma (IFNγ) and tumor necrosis factor α (TNFα) by $CD4^+$ and $CD8^+$ T cells was increased upon oncolytic virus treatment, with no difference being observed between oHSV and oHSV-IpaH9.8 (Figures 7H and 7I). These data indicate that oncolytic HSV-1 armed with IpaH9.8 promotes tumor T cell infiltration and induces stronger antitumor activity.

DISCUSSION

Cancer immunotherapy exemplified by immune checkpoint blockade has revolutionized cancer treatment.[1] However, only 20%–30% of cancer patients respond to current immune checkpoint inhibitors (ICIs). Hot tumors with sufficient immune cell infiltration tend to be more responsive to ICI treatment. By contrast, cold tumors with scarce immune cell infiltration are refractory to the treatment.[2,3] Combination therapies are effective means to overcome the conundrum of ICI resistance. Among the combination strategies, oncolytic virus has gained extensive attention due to its remarkable ability to "heat up" tumors, thereby converting cold tumors into hot ones.[4,31]

Oncolytic viruses are WT or genetically engineered viruses that selectively replicate in tumor cells. OV replication results in highly inflammatory cancer cell death and overturns the immunosuppressive state of the tumor microenvironment.[4] These benefits have rendered OV a

Figure 3. GBP1 restricts HSV-1 replication by blocking viral genome nuclear translocation

(A) HT1080 control or GBP1-overexpressing cells were infected with HSV-1 (MOI = 1), and the expression of viral genes (*ICP0*, *UL23*) was determined by RT-qPCR at the indicated time points post-infection. (B) HT1080 control or GBP1 stable cells were infected with HSV-1 (MOI = 5) for 1 h at 4°C, and then another 1 h at 37°C in the presence of cycloheximide (100 μg/mL). The relative viral genome copy number was quantified by qPCR. (C) HT1080 control or GBP1 stable cells were infected with HSV-1 (MOI = 5) for 1 h at 4°C and then another 3 h at 37°C in the presence of cycloheximide (100 μg/mL). Nuclear fractions were isolated from the infected cells and the relative viral genome copy number was quantified by qPCR. (D) HT1080 control or GBP1 knockout cells were infected with HSV-1 (MOI = 5) for 1 h at 4°C and then another 3 h at 37°C in the presence of cycloheximide (100 μg/mL). Nuclear fractions were isolated from the infected cells, and the relative viral genome copy number was quantified by qPCR. (E) U2OS control or GBP1 stable cells were infected with HSV-1 (MOI = 50) for 1 h at 4°C and then another 3 h at 37°C in the presence of cycloheximide (100 μg/mL). ICP5 and FLAG-GBP1 were detected by immunofluorescence staining. Scale bars, 20 μm. (F) The percentage of cells with perinuclear localization of ICP5 in (E) was quantified. (G) U2OS control or GBP1 stable cells were mock-infected or infected with EdC-labeled HSV-1 (MOI = 50) for 1 h at 4°C and then another 3 h at 37°C in the presence of cycloheximide (100 μg/mL). Nuclei were stained with DAPI, and viral genome was visualized by click chemistry. Scale bars, 20 μm. (H) Statistical analysis represents the percentage of viral nuclear genome per cell in (G). (I) U2OS control or GBP1 knockout cells were infected with EdC-labeled HSV-1 (MOI = 50) for 1 h at 4°C and then another 3 h at 37°C in the presence of cycloheximide (100 μg/mL). Statistical analysis represents the percentage of viral nuclear genome per cell. Data are presented as means ± SEM, and statistical analyses were performed using a two-tailed unpaired Student's t test. Data are representative of three independent experiments. *$p < 0.05$; **$p < 0.01$; ***$p < 0.005$; ***$p < 0.001$; N.S., not significant.

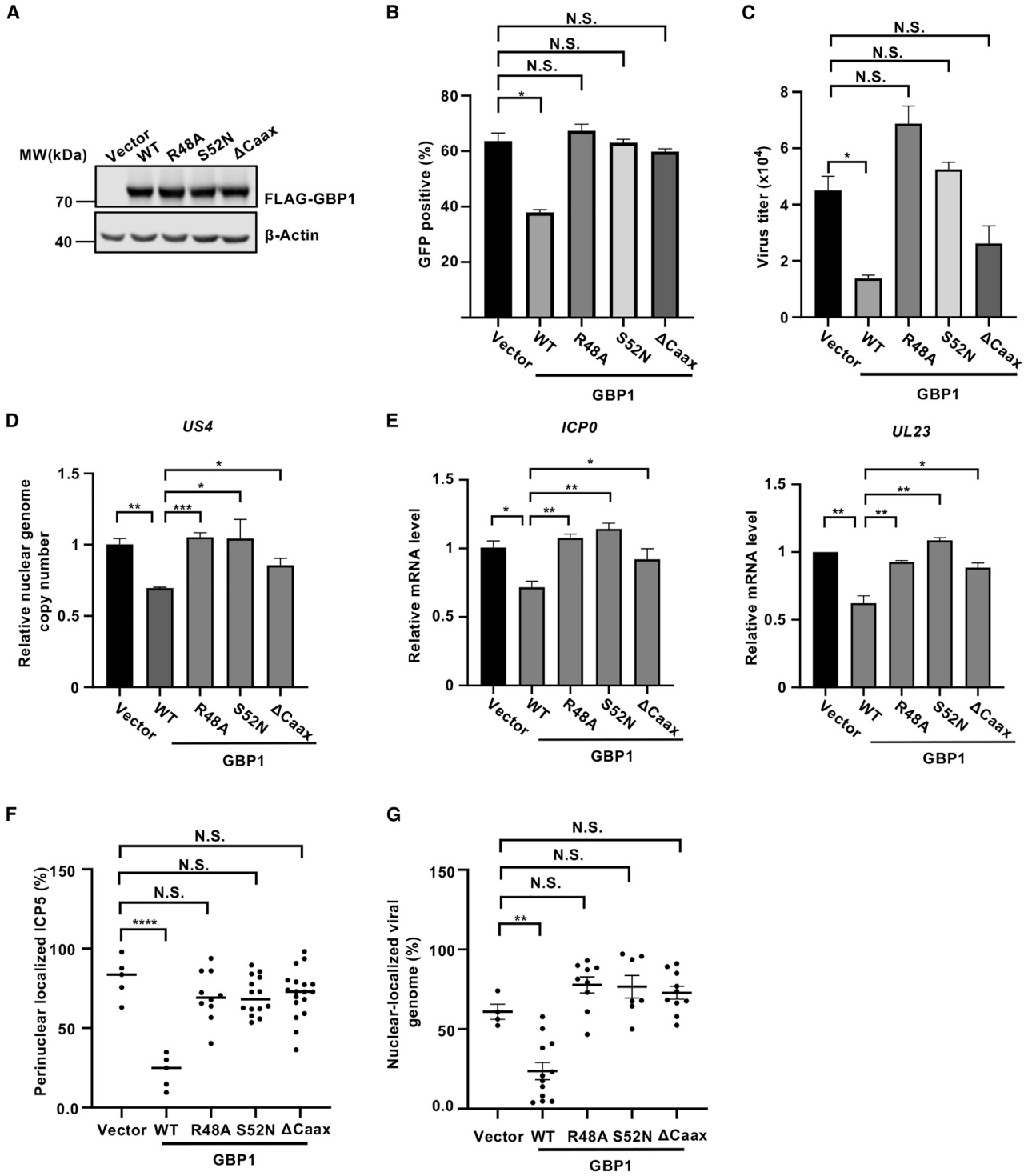

Figure 4. The GTPase activity and prenylation of GBP1 are required to restrict HSV-1 replication

(A) HT1080 cells were transduced with control vector, GBP1, or the indicated mutants to generate stable cells. Whole-cell lysates were analyzed by immunoblotting. (B) HT1080 stable cells as described in (A) were infected with GFP-HSV-1 (MOI = 0.01), and the GFP-positive cell percentage was quantified by flow cytometry at 24 h post-infection. Viral titer in the culture medium was determined by plaque assay at 24 h post-infection (C). (D) HT1080 stable cells were infected with HSV-1 (MOI = 5) for 1 h at 4°C and then another 3 h at 37°C in the presence of cycloheximide (100 μg/mL). Nuclear viral genome was determined by qPCR at 3 h post-infection. (E) HT1080 stable cells were

(legend continued on next page)

perfect partner for the development of combination therapies with ICIs. Among the different OV types, oncolytic HSV-1 has gained momentum by showing promising effects in the treatment of melanoma and other cancer types, leading to its regulatory approval for the treatment of advanced melanoma in the United States, Europe, and Australia.[6] Despite these advantages, the efficacy of OV as monotherapy is limited. For example, the response rate of T-VEC monotherapy is around 16% in melanoma patients, indicating that there is great room for improvement.[9]

To improve OV efficacy, tremendous efforts have been made to optimize the transgenes carried by OVs. The transgenes encoded by OVs can be roughly divided into cytokines, immune checkpoint blockers, T cell engagers, and TAAs.[4] For example, GM-CSF and Interleukin-12 (IL-12) are cytokines that have been extensively studied as transgenes to stimulate antitumor immunity. GM-CSF stimulates the maturation and activation of DCs to augment antitumor immunity. The durable response rate of T-VEC encoding GM-CSF is around 10-fold compared with that of recombinant GM-CSF.[4] IL-12 is a Th1 cytokine that polarizes naive T cells into Th1 cells to enhance antitumor immunity, and is encoded in multiple types of OVs, including oncolytic HSV-1, vaccinia virus, and adenovirus, to improve cancer immunotherapy.[32–35] Oncolytic viruses carrying immune checkpoint antibodies, such as PD1 and PD-L1 blocking antibodies as well as PD-L1 inhibitory proteins, have shown promising results in preclinical mouse models.[36–38] Moreover, TAAs (e.g., HER2 for breast cancer treatment) and T cell engagers (e.g., bispecific T cell engagers that bind CD3 and a surface antigen of cancer cells) are being developed to improve OV therapies.[4] However, while these modifications primarily focus on modulating the host response, the improvement of OV replication has received less attention. Taking T-VEC as an example, ICP34.5 has been identified as a major virulence factor contributing to HSV1 neuropathogenesis, so it is depleted in T-VEC to reduce neurovirulence and improve medication safety.[39] As a multifunctional viral protein, ICP34.5 plays a critical role in viral immune evasion.[39,40] Furthermore, ICP34.5 antagonizes autophagy to facilitate viral replication.[12] Depletion of ICP34.5 reduces neurovirulence of oHSV-1, but also renders the modified virus attenuated and unable to replicate efficiently in the harsh tumor microenvironment. We postulate that targeting restriction factors of OV may improve viral replication to improve OV therapeutic efficacy.

Previous studies have revealed that augmenting the replication of oncolytic HSV-1 can improve its antitumor activity. For example, the FDA-approved proteasome inhibitor Bortezomib can induce HSP90, which promotes the nuclear localization of HSV-1 polymerase and increases viral replication. Oncolytic HSV-1 combined with Bortezomib has resulted in synergistic antitumor effects.[41] In addition, HDAC6 inhibition can counteract the antiviral effect of type I interferons and increase the shuttling of oHSV to the nucleus rather than the lysosome, leading to increased oHSV replication.[42] ENT1 antagonists, which increase cellular ribonucleoside activity, have also been shown to promote oHSV replication in cancer cells.[43] Our study defines GBP1 as a restriction factor against HSV-1 and reveals that GBP1 remodels actin cytoskeletal organization of infected cells to impede the trafficking of HSV-1 capsid. We take advantage of a well-defined bacterial GBP1-degrading protein IpaH9.8 to engineer an oncolytic HSV-1 armed with IpaH9.8 (oHSV-IpaH9.8). oHSV-IpaH9.8 effectively induces GBP1 degradation and ablates the antiviral activity of GBP1. Importantly, oHSV-IpaH9.8 shows stronger antitumor immunity, demonstrating that our strategy of targeting GBP1 to improve OV therapeutic efficacy works. Whether similar strategies can be applied to disarm other antiviral restriction factors to further promote OV replication warrants further investigation.

In summary, our study has identified GBP1 as a restriction factor against HSV-1. GBP1 modulates the cytoskeleton of infected cells to impede the nuclear entry of HSV-1 genome. Oncolytic HSV-1 encoding a bacterial GBP1 degrader IpaH9.8 effectively antagonizes GBP1 and shows superior antitumor activity. Our study features a strategy for improving the replication of OVs by targeting restriction factors and holds great promise for achieving improved therapeutic efficacy in cancer treatment.

MATERIALS AND METHODS

Cell culture

HT1080 (kindly provided by Drs. Hong-Bing Shu and Qing Yang, Wuhan University), MC38 (kindly provided by Dr. Jinfang Zhang, Wuhan University), HEK293T, U2OS, and VERO (ATCC) cells were cultured in Dulbecco's modified Eagle's medium (DMEM) (Sigma) supplemented with 10% fetal bovine serum (FBS) (LONSERA, Shanghai, China) and 1% penicillin-streptomycin (HyClone). THP1 cells (ATCC) were cultured in RPMI 1640 (Sigma) supplemented with 10% FBS (LONSERA, Shanghai, China) and 1% penicillin-streptomycin (HyClone). All cell lines were routinely tested for mycoplasma contamination and mycoplasma-negative cells were used in the study.

Mouse experiments

All mouse experiments were approved by the Institutional Animal Care and Ethics Committee of the Medical Research Institute, Wuhan University. C57BL/6J mice were purchased from Hu'nan SJA Laboratory Animal Co., Ltd (Changsha, China) and kept in a specific pathogen-free facility at the Medical Research Institute, Wuhan University.

infected with HSV-1 (MOI = 5), and viral gene expression was quantified by RT-qPCR at 6 h post-infection. (F) U2OS stable cells were mock-infected or infected with HSV-1 (MOI = 50) for 1 h at 4°C and then another 3 h at 37°C in the presence of cycloheximide (100 μg/mL), followed by ICP5 immunostaining. The percentage of cells with perinuclear localization of ICP5 was quantified. (G) U2OS stable cells were mock-infected or infected with EdC-labeled HSV-1 (MOI = 50) for 1 h at 4°C and then another 3 h at 37°C in the presence of cycloheximide (100 μg/mL), followed by click chemistry to visualize viral genome. Data are presented as means ± SEM, and statistical analyses were performed using a two-tailed unpaired Student's t test. Data are representative of three independent experiments. *$p < 0.05$; **$p < 0.01$; ***$p < 0.005$; ****$p < 0.001$; N.S., not significant.

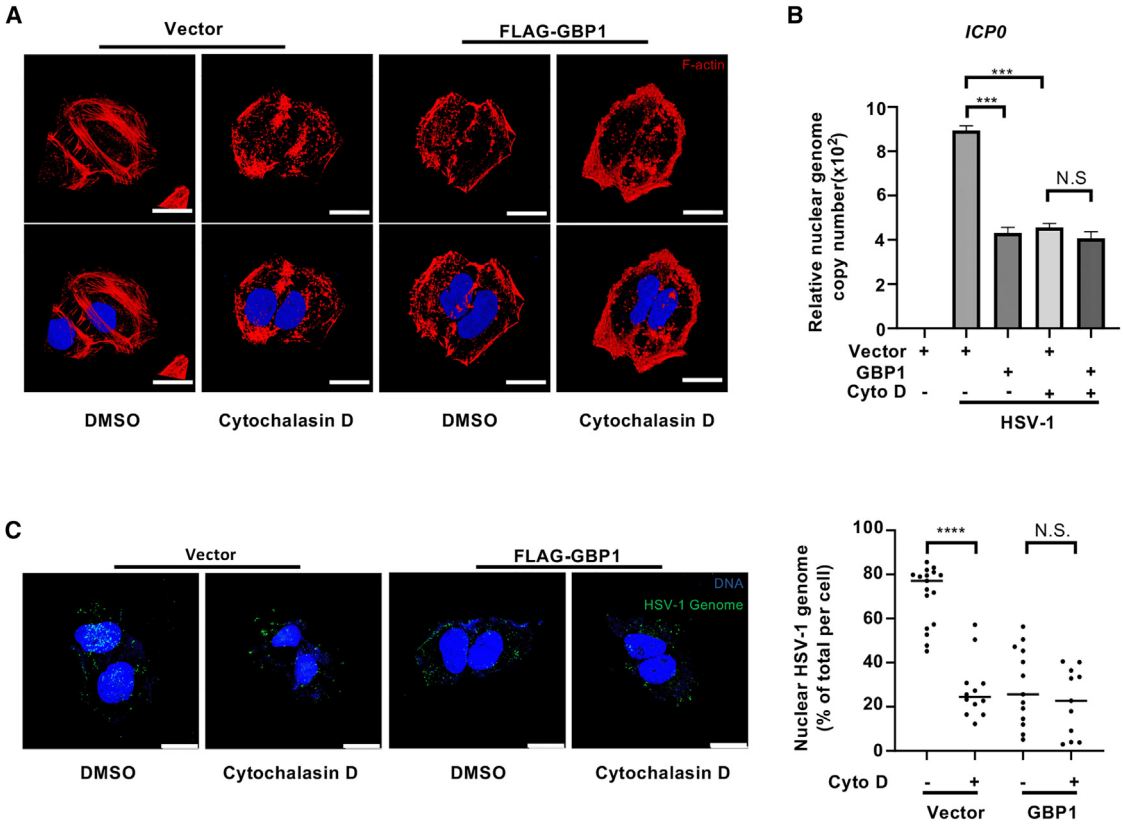

Figure 5. GBP1 disrupts actin filament formation

(A) U2OS control or GBP1 stable cells were mock-treated or treated with cytochalasin D (200 nM). The stable cells were fixed at 3 h post-treatment and actin was visualized by phalloidin staining. Scale bars, 20 μm. (B) HT1080 control or GBP1 stable cells were mock-treated, or treated with cytochalasin D (200 nM), and infected with HSV-1 (MOI = 5) in the presence of cycloheximide (100 μg/mL). Nuclear viral genomes were quantified by qPCR at 3 h post-infection. (C) U2OS control or GBP1 stable cells treated with DMSO or cytochalasin D (200 nM) were mock-infected or infected with EdC-labeled HSV-1 (MOI = 50) in the presence of cycloheximide (100 μg/mL). The cells were fixed at 3 h post-infection and viral genomes were visualized by click chemistry. Scale bars, 20 μm. Data are presented as means ± SEM, and statistical analyses were performed using a two-tailed unpaired Student's t test. Data are representative of three independent experiments. ***$p < 0.005$; ****$p < 0.001$; N.S., not significant.

MC38 cells (1×10^5) were re-suspended in 75 μL of ice-cold PBS and mixed with 25 μL of Matrigel (356231, Corning) and 100 μL of the suspension was injected subcutaneously into the left flank of C57BL/6J mice. Tumor size was measured every other day, and tumor volume was calculated using the formula $V = (L \times W^2)/2$, with L and W denoting the widest and the smallest diameter, respectively. When tumor volume reached ~100 mm^3 (day 7 after implantation), the mice received 10^6 pfu of HSV-1Δ34.5/Δ47 or HSV-1Δ34.5/Δ47-IpaH9.8 via intratumoral injection, and the injection was repeated every other day for a total of five times. Tumor-bearing mice were killed on day 18 after implantation and tumors were collected and processed for further analysis.

Viruses

HSV-1 and GFP-HSV-1 (F strain) was propagated using VERO cells, and virus titer was measured by standard plaque assay using VERO cells.[19] HSV-1Δ34.5/Δ47 and HSV-1Δ34.5/Δ47-IpaH9.8 were generated by two-step Red-mediated recombination and propagated and titrated using VERO cells.

EdC genome-labeled HSV-1 was generated as previously described.[44] Briefly, VERO cells cultured in DMEM containing 2% FBS were infected with HSV-1 (MOI = 0.01), then EdC (#9075-47-4, Aladdin, Shanghai, China) was added at 4 h post-infection to a final concentration of 5 μM. Culture supernatant was harvested at 48 h post-infection and virus titer was determined by plaque assay.

Plasmids

For transient expression in mammalian cells, pCS2-FLAG-GBP1-5 and pCS2-FLAG-IpaH9.8 were kindly provided by Dr. Feng Shao (National Institute of Biological Sciences, Beijing).

For stable cell line generation, GBP1 and its mutants were constructed into pCDH-CMV-EF1α-Puro or pCDH-CMV-EF1α-Hygro (System Biosciences). Single guide RNA (sgRNA) targeting GBP1-5 was

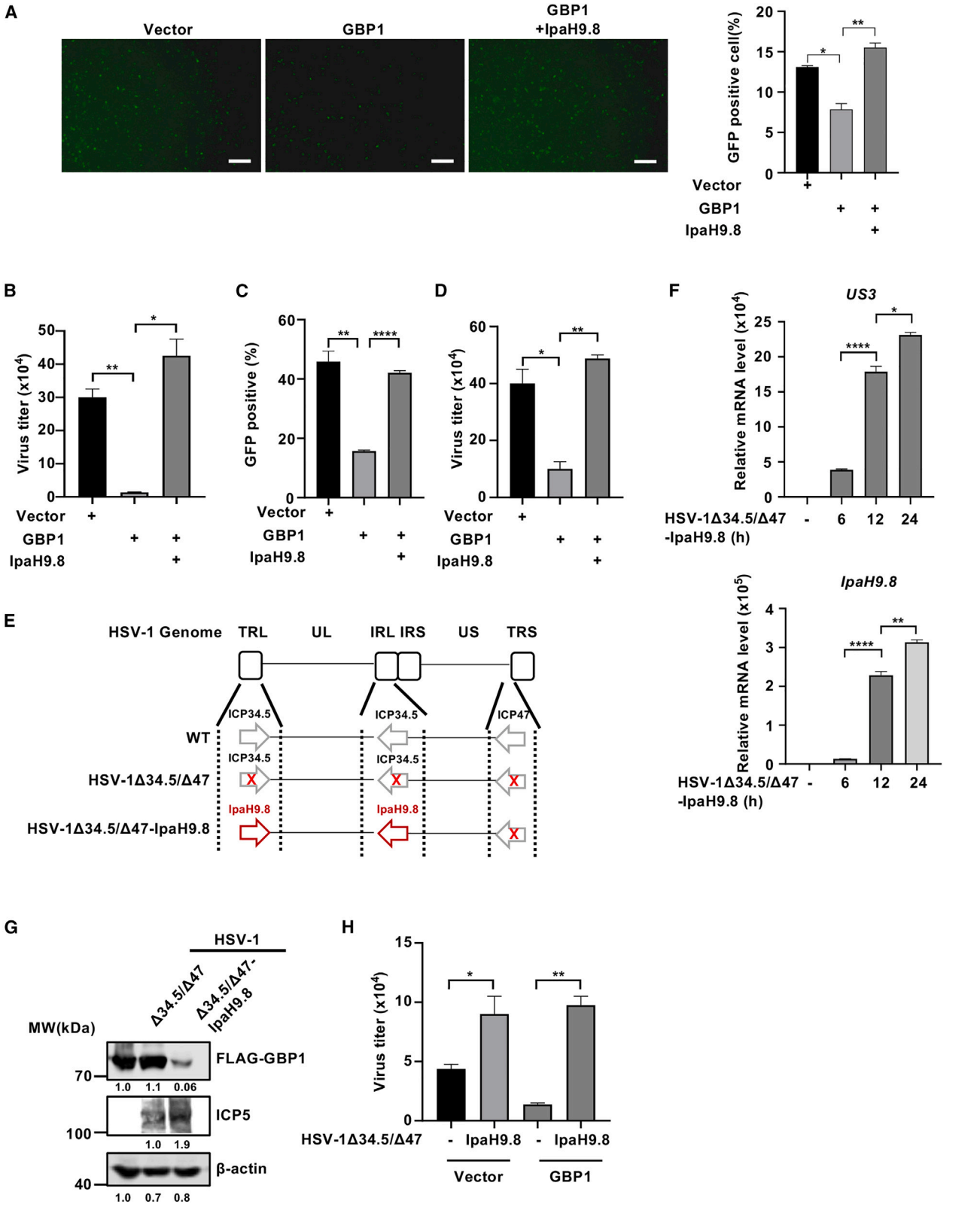

(legend on next page)

inserted into Lenti-CRISPRv2 (#52961, Addgene). The sgRNA sequences are listed in Table S1.

Lymphocyte isolation

Single-cell suspensions were prepared from spleens and tumors. Briefly, spleens were mechanically disrupted, and splenocytes were re-suspended in cold PBS. Red blood cells (RBCs) were lysed with RBC lysis buffer (BL503B, Biosharp, Hefei, China) for 3 min at room temperature. Then 1 mL of RPMI 1640 supplemented with 10% FBS was added to stop the reaction. The cell suspensions were filtered through a nylon mesh strainer (45 μm), and the cells were harvested and re-suspended in PBS for further analysis.

For isolation of tumor-infiltrating lymphocytes, tumor tissue was cut into small pieces (1–2 mm in diameter). The tumor pieces were then minced in cold PBS and the suspensions were passed through a 70-μm cell strainer. The cell strainer was rinsed twice with cold PBS to collect all cells. The collected cells were re-suspended in 3 mL of 40% Percoll (BS909, Biosharp, Hefei, China) and transferred into a 15 mL tube, laid slowly on 3 mL of 80% Percoll, and centrifuged at 1,400 × *g* for 15 min at 4°C. The lymphocytes at the interface of 40% and 80% Percoll were collected and re-suspended in staining buffer. The isolated lymphocytes were counted and used for further staining analysis.

Flow cytometry

FITC anti-mouse CD3 (#100204, 1:200), Pacific Blue anti-mouse CD4 (#100531, 1:200), PerCP/Cyanine5.5 anti-mouse CD4 (#100434, 1:200), FITC anti-mouse CD8a (#100706, 1:200), PE/Cyanine7 anti-mouse CD8a (#100722, 1:200), APC anti-mouse IFN-γ (#505810, 1:200), PE anti-mouse TNF-α (#506306, 1:200), PE anti-mouse CD366 (Tim-3) (#119704, 1:200), and APC anti-mouse CD279 (PD-1) (#135210, 1:200) were ordered from Biolegend.

For intracellular cytokine staining, lymphocytes (1×10^6) were stimulated with 50 ng/mL of PMA (phorbol 12-myristate 13-acetate) (#P8139, Sigma) and 1 μM of ionomycin (#13909, Sigma) in the presence of brefeldin A (#S7046, Selleck) (5 μg/mL) for 4 h. Then the stimulated cells were fixed and permeabilized with Fixation Buffer (#420801, Biolegend) for 20 min at 4°C, and stained with fluorochrome-conjugated antibody cocktails for 15 min at 4°C. Flow cytometry data were acquired on BD LSRFortessa X-20 and analyzed with FlowJo software.

Generation of oncolytic HSV-1 Δ34.5/Δ47-IpaH9.8

ICP34.5- and ICP47-deficient HSV-1 (strain F) was generated by deleting the coding sequences of ICP34.5 and ICP47 in a bacterial artificial chromosome (BAC) through two-step Red-mediated recombination.[45,46] Briefly, a linear DNA fragment containing a kanamycin resistance expression cassette, an I-SceI restriction enzyme site, and flanking sequences derived from HSV-1 genomic DNA were PCR-amplified (primers are listed in Table S1). The DNA fragment was then purified and electroporated into GS1783 cells harboring HSV-1 BAC to induce the first round of recombination. The correct recombination of the KanR/I-SceI cassette was verified by PCR amplification of the purified BAC DNA. The GS1783 strain containing the modified HSV-1 BAC was then incubated with 1% L-arabinose (Sigma-Aldrich) to induce the expression of I-SceI. A second round of Red-mediated recombination led to the depletion of the KanR/I-SceI cassette. Kanamycin-sensitive and chloramphenicol-resistant colonies were picked, and HSV-1 BAC DNA was extracted from GS1783 bacteria. The successful deletion of the target genes was verified by PCR amplification of the purified BAC DNA and Sanger sequencing. ICP34.5- and ICP47-deficient HSV-1 was named HSV-1Δ34.5/Δ47.

HSV-1Δ34.5/Δ47 expressing IpaH9.8 was generated by inserting the coding sequence of IpaH9.8 into the coding region of ICP34.5 through two-step Red-mediated recombination as described above. The successful insertion of the target gene was verified by PCR amplification and Sanger sequencing. HSV-1Δ34.5/Δ47 expressing IpaH9.8 was named HSV-1Δ34.5/Δ47-IpaH9.8.

For the generation of OVs, BAC DNA (~2 μg) was transfected into VERO cells (1.5×10^5) using Fugene HD (Promega, Wisconsin, United States). Viruses were harvested when 100% of the cells displayed pronounced cytopathic effects at 3–5 days post-transfection. HSV-1Δ34.5/Δ47 and HSV-1Δ34.5/Δ47-IpaH9.8 were titrated by standard plaque assay using VERO cells.

Viral entry assay

HT1080 cells were inoculated with HSV-1 (MOI = 5) in infection medium (DMEM, 25 mM HEPES pH 7.5, 100 U/mL penicillin, 100 μg/mL streptomycin, 0.2% bovine albumin fraction V) for 60 min at 4°C in presence of cycloheximide (100 μg/mL). The infected cells were washed twice with PBS and incubated in fresh infection medium with cycloheximide (100 μg/mL) at 37°C

Figure 6. Oncolytic HSV-1 armed with IpaH9.8 effectively degrades GBP1 and promotes virus replication

HEK293T cells were transfected with the indicated plasmids. After 24 h, the transfected cells were infected with GFP-HSV-1 (MOI = 0.01). GFP expression was imaged at 36 h post-infection (Scale bars, 100 μm), and the GFP-positive cell percentage was quantified by flow cytometry (A). Viral titer in the medium was determined by plaque assay at 36 h post-infection (B). (C) HT1080 stable cells were infected with GFP-HSV-1 (MOI = 0.01). The GFP-positive cell percentage was quantified by flow cytometry at 24 h post-infection. Viral titer in the medium was determined by plaque assay at 24 h post-infection (D). (E) Schematic representation of the viruses used in the study (HSV-1 Δ34.5/Δ47 [oHSV]; HSV-1 Δ34.5/Δ47-IpaH9.8 [oHSV-IpaH9.8]). (F) HT1080 cells were infected with oHSV-IpaH9.8 (MOI = 1), and the expression of the indicated genes was determined by RT-qPCR at the indicated time points. (G) HT1080 FLAG-GBP1 stable cells were mock-infected or infected with oHSV or oHSV-IpaH9.8 (MOI = 1). Whole-cell lysates were analyzed by immunoblotting at 16 h post-infection. Viral titer in the medium was determined by plaque assay at 16 h post-infection (H). Data are presented as means ± SEM, and statistical analyses were performed using a two-tailed unpaired Student's t test. Data are representative of three independent experiments. *$p < 0.05$; **$p < 0.01$; ****$p < 0.001$; N.S., not significant.

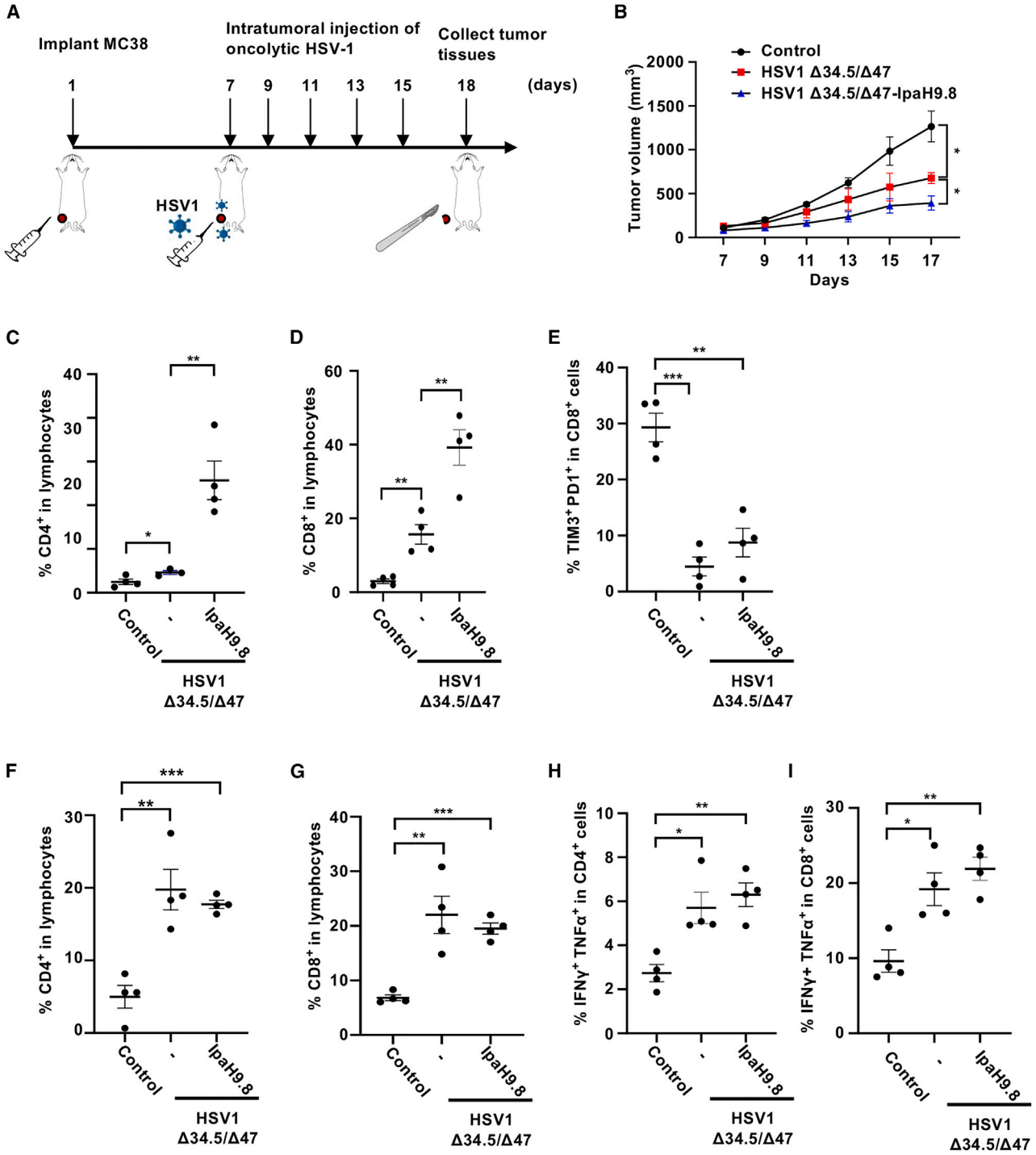

Figure 7. Oncolytic HSV-1 armed with IpaH9.8 demonstrates stronger antitumor activity

(A) Workflow for the MC38 colorectal tumor model and oncolytic virus treatment. (B) Tumor volume was quantified at the indicated time points. (C)–(E) Flow cytometry analysis of tumor-infiltrating $CD4^+$, $CD8^+$, and $TIM3^+PD1^+CD8^+$ T cells. (F) and (G) Flow cytometry analysis of $CD8^+$ and $CD4^+$ T cells in the spleens of the MC38 tumor-bearing mice. (H) and (I) Mouse splenocytes were stimulated with PMA and ionomycin for 4 h, followed by flow cytometry analysis of $IFN\gamma^+TNF\alpha^+CD4^+$ and $IFN\gamma^+TNF\alpha^+CD8^+$ T cells. Tumor volume $V = (L \times W^2)/2$, where L and W denote the widest and the smallest diameter, respectively. Data are presented as means ± SEM, and statistical analyses were performed using a two-tailed unpaired Student's t test or the log rank test (B). Data are representative of three independent experiments. *$p < 0.05$; **$p < 0.01$; ***$p < 0.005$; N.S., not significant.

for 1 h. Then genomic DNA was extracted, and HSV-1 genome copy number was quantified by qPCR. The qPCR primers are listed in Table S1.

RNA extraction and qRT-PCR

THP1 or HT1080 cells were infected with HSV-1 (MOI = 5) for 8 h. Total RNA was extracted using TRIzol reagent (#9109, Takara). One microgram of total RNA was used for reverse transcription with a HiScript II first Strand cDNA Synthesis Kit (Vazyme, Nanjing, China) according to the manufacturer's instructions. The cDNA mixture was diluted 20 times and was then subjected to qRT-PCR analysis with SYBR green qPCR master mix (Monad, Suzhou, China). The relative expression of the target genes was normalized to the expression of *ATCB*.

The primer sequences for qRT-PCR are provided in Table S1.

HSV-1 nuclear genome copy number quantification

HT1080 cells were inoculated with HSV-1 (MOI = 5) in infection medium (DMEM, 25 mM HEPES pH 7.5, 100 U/mL penicillin, 100 μg/mL streptomycin, 0.2% bovine albumin fraction V) for 1 h at 4°C in presence of cycloheximide (100 μg/mL) (#5142-23-4, MCE). Then the infected cells were washed twice with PBS and incubated in fresh infection medium containing cycloheximide (100 μg/mL) for 3 h at 37°C. After another two washing steps with ice-cold PBS, cytoplasmic and nuclear fractions were prepared as previously described.[44] Nuclear DNA was extracted with a TIANamp Genomic DNA kit (DP304-03, TIANGEN, Beijing, China) according to the manufacturer's instructions. HSV-1 genome copy number was quantified by qPCR and TERT was used as an internal control. The primer sequences for qPCR are provided in Table S1.

Immunofluorescence

U2OS cells were inoculated with HSV-1 (MOI = 50) in infection medium for 60 min at 4°C in presence of cycloheximide (100 μg/mL). The infected cells were washed twice with PBS and incubated in fresh infection medium with cycloheximide (100 μg/mL) at 37°C for 3 h. The cells were then fixed with 4% (w/v) paraformaldehyde (#DF0131, LEAGENE) for 10 min, followed by permeabilization with 1% Triton X-100 for 5 min. After blocking with 10% goat serum in PBS for 1 h at room temperature, the fixed cells were incubated with mouse anti-HSV-1 ICP5 antibody (Santa Cruz, sc-56989, 1:50) at 4°C overnight. For GBP1 detection, the samples were incubated with rabbit anti-DYKDDDDK polyclonal antibody (Proteintech, 20543-1-AP, 1:100) at 4°C overnight, followed by incubation with goat anti-mouse polyclonal secondary antibody (Alexa Fluor 488, Invitrogen #A10680, 1:1000) or anti-rabbit secondary antibody (Alexa Fluor 594, Invitrogen #A11012, 1:1000) at room temperature for 1 h. Slides were then mounted with DAPI Fluoromount (#36308ES20, Yeasen, Shanghai, China) according to the manufacturer's instructions. Images were collected with a confocal microscope (Leica Stellaris 5), the pictures were processed using Leica image browser, and quantification was performed with ImageJ (NIH).

Immunoblotting

Transfected or infected cells were collected at the indicated time points and lysed with NP-40 buffer (50 mM Tris-HCl pH 7.4, 150 mM NaCl, 1% NP-40, 1 mM EDTA, 5% glycerol) supplemented with a protease inhibitor cocktail as previously described.[20] Centrifuged cell lysates were boiled with 1x sodium dodecyl sulfate (SDS) sample buffer at 95°C for 10 min. The samples were separated by SDS-polyacrylamide gel electrophoresis and analyzed by immunoblotting.

The following commercial antibodies were used for immunoblotting in this study:

- mouse anti-HA monoclonal antibody (#2063, Dia-An Biotechnology, Wuhan, China) (1:5,000)
- anti-DYKDDDDK monoclonal antibody (#2064, Dia-An Biotechnology, Wuhan, China) (1:5,000)
- anti-β-actin monoclonal antibody (#2060, Dia-An Biotechnology, Wuhan, China) (1:5,000)
- anti-VP16 monoclonal antibody (# SC-7545, Santa Cruz) (1:1,000)
- anti-GBP1 monoclonal antibody (# SC-53857, Santa Cruz) (1:1,000)
- anti-ICP5 monoclonal antibody (# SC-56989, Santa Cruz) (1:1,000)
- IRDye 800CW goat anti-mouse immunoglobulin (Ig)G (#926–32210, LI-COR Biosciences, 1:10,000)
- IRDye 800CW goat anti-rabbit IgG (#926–32211, LI-COR Biosciences, 1:10,000)

Analysis of HSV-1 genome localization by click chemistry

U2OS cells were inoculated with EdC-labeled HSV-1 (MOI = 50) for 1 h at 4°C in presence of cycloheximide (100 μg/mL). Then the cells were washed twice with PBS, and incubated in infection medium with cycloheximide (100 μg/mL) at 37°C for 3 h. The samples were fixed immediately with 4% (w/v) PFA in PBS for 10 min and permeabilized with 1% Triton X-100 for 5 min at room temperature. Viral genomes were visualized using copper(I)-catalyzed azide alkyne cycloaddition as previously described.[47] Briefly, the fixed samples were incubated with freshly prepared click chemistry staining mix (10 μM AZDye 488-azide [#1475-1, Click Chemistry Tools], 1 mM CuSO4 [#7758-99-8, Sinopharm Chemical Reagent Co., Shanghai], 10 mM sodium ascorbate [#S105026, Aladdin, Shanghai], 10 mM amino-guanidine [#A151036, Aladdin, Shanghai], and 1 mM THPTA [#760952-88-3, Click Chemistry Tools]). DAPI staining and slide mounting were performed as described in the immunofluorescence section. Images were acquired with a confocal microscope (Leica Stellaris 5) and analysis was performed with ImageJ (NIH).

Statistical analysis

Data represent the mean of at least three independent experiments, and error bars denote standard error of the mean (SEM). A two-tailed Student's t test or analysis of variance was used for statistical analysis,

and the log rank test applied to Figure 7B was performed in GraphPad 7, *p < 0.05, **p < 0.01, ***p < 0.005, ****p < 0.0001, N.S, not statistically significant.

DATA AVAILABILITY

All data are available in the main text or the supplemental information. RNA sequencing data were uploaded to the GEO database (accession number: GSE114966).

SUPPLEMENTAL INFORMATION

Supplemental information can be found online at https://doi.org/10.1016/j.omto.2023.04.006.

ACKNOWLEDGMENTS

We thank Drs. Jinfang Zhang, Hong-Bing Shu, Qing Yang, Zheng Liu (Wuhan University), Feng Shao (National Institute of Biological Sciences, Beijing), Pinghui Feng (University of Southern California), and Gregory A. Smith (Northwestern University) for reagents and suggestions. J.Z. is supported by the National Key Research and Development Program of China (2021YFC2701800, 2021YFC2701804), a startup fund from Wuhan University, grants from the National Natural Science Foundation of China (31970156 and 82172261), the Fundamental Research Funds for the Central Universities (2042022dx0003), and the Open Research Fund Program of the State Key Laboratory of Virology of China (2022KF010 to Q.Q.). We thank the core facility of the Medical Research Institute at Wuhan University for excellent technical support and thank Professor Stanley Lin (Shantou University Medical College) for proofreading our manuscript.

AUTHOR CONTRIBUTIONS

J.X., J.Z., Z.S., and K.L. designed and supervised the study; J.X., S.W., and Y.Z. performed most experiments; M.G., X.T., and L.Z. helped with some experiments; D.P. provided critical reagents and helped with data analysis; Q.Q. helped with funding acquisition and data analysis; J.Z. and J.X. wrote the paper; all the authors approved the manuscript.

DECLARATION OF INTERESTS

The authors declare no competing interests.

REFERENCES

1. Waldman, A.D., Fritz, J.M., and Lenardo, M.J. (2020). A guide to cancer immunotherapy: from T cell basic science to clinical practice. Nat. Rev. Immunol. *20*, 651–668. https://doi.org/10.1038/s41577-020-0306-5.

2. Vesely, M.D., Zhang, T., and Chen, L. (2022). Resistance mechanisms to anti-PD cancer immunotherapy. Annu. Rev. Immunol. *40*, 45–74. https://doi.org/10.1146/annurev-immunol-070621-030155.

3. Jenkins, R.W., Barbie, D.A., and Flaherty, K.T. (2018). Mechanisms of resistance to immune checkpoint inhibitors. Br. J. Cancer *118*, 9–16. https://doi.org/10.1038/bjc.2017.434.

4. Twumasi-Boateng, K., Pettigrew, J.L., Kwok, Y.Y.E., Bell, J.C., and Nelson, B.H. (2018). Oncolytic viruses as engineering platforms for combination immunotherapy. Nat. Rev. Cancer *18*, 419–432. https://doi.org/10.1038/s41568-018-0009-4.

5. Su, W., Qiu, W., Li, S.J., Wang, S., Xie, J., Yang, Q.C., Xu, J., Zhang, J., Xu, Z., and Sun, Z.J. (2023). A dual-responsive STAT3 inhibitor nanoprodrug combined with oncolytic virus elicits synergistic antitumor immune responses by igniting pyroptosis. Adv. Mater. *35*, e2209379. https://doi.org/10.1002/adma.202209379.

6. Rehman, H., Silk, A.W., Kane, M.P., and Kaufman, H.L. (2016). Into the clinic: talimogene laherparepvec (T-VEC), a first-in-class intratumoral oncolytic viral therapy. J. Immunother. Cancer *4*, 53. https://doi.org/10.1186/s40425-016-0158-5.

7. Andtbacka, R.H.I., Collichio, F., Harrington, K.J., Middleton, M.R., Downey, G., Öhrling, K., and Kaufman, H.L. (2019). Final analyses of OPTiM: a randomized phase III trial of talimogene laherparepvec versus granulocyte-macrophage colony-stimulating factor in unresectable stage III-IV melanoma. J. Immunother. Cancer *7*, 145. https://doi.org/10.1186/s40425-019-0623-z.

8. Kaufman, H.L., Andtbacka, R.H.I., Collichio, F.A., Amatruda, T., Senzer, N.N., Chesney, J., Delman, K.A., Spitler, L.E., Puzanov, I., Ye, Y., et al. (2014). Primary overall survival (OS) from OPTiM, a randomized phase Ill trial of talimogene laherparepvec (T-VEC) versus subcutaneous (SC) granulocyte-macrophage colony-stimulating factor (GM-CSF) for the treatment (tx) of unresected stage IIIB/C and IV melanoma. J. Clin. Oncol. *32*, 9008a. https://doi.org/10.1200/jco.2014.32.15_suppl.9008a.

9. Ferrucci, P.F., Pala, L., Conforti, F., and Cocorocchio, E. (2021). Talimogene laherparepvec (T-VEC): an intralesional cancer immunotherapy for advanced melanoma. Cancers *13*, 1383. https://doi.org/10.3390/cancers13061383.

10. Kanai, R., Zaupa, C., Sgubin, D., Antoszczyk, S.J., Martuza, R.L., Wakimoto, H., and Rabkin, S.D. (2012). Effect of gamma34.5 deletions on oncolytic herpes simplex virus activity in brain tumors. J. Virol. *86*, 4420–4431. https://doi.org/10.1128/JVI.00017-12.

11. Mossman, K.L., and Smiley, J.R. (2002). Herpes simplex virus ICP0 and ICP34.5 counteract distinct interferon-induced barriers to virus replication. J. Virol. *76*, 1995–1998. https://doi.org/10.1128/jvi.76.4.1995-1998.2002.

12. Orvedahl, A., Alexander, D., Tallóczy, Z., Sun, Q., Wei, Y., Zhang, W., Burns, D., Leib, D.A., and Levine, B. (2007). HSV-1 ICP34.5 confers neurovirulence by targeting the Beclin 1 autophagy protein. Cell Host Microbe *1*, 23–35. https://doi.org/10.1016/j.chom.2006.12.001.

13. Kurokawa, C., Iankov, I.D., Anderson, S.K., Aderca, I., Leontovich, A.A., Maurer, M.J., Oberg, A.L., Schroeder, M.A., Giannini, C., Greiner, S.M., et al. (2018). Constitutive interferon pathway activation in tumors as an efficacy determinant following oncolytic virotherapy. J. Natl. Cancer Inst. *110*, 1123–1132. https://doi.org/10.1093/jnci/djy033.

14. Ngo, C.C., and Man, S.M. (2017). Mechanisms and functions of guanylate-binding proteins and related interferon-inducible GTPases: roles in intracellular lysis of pathogens. Cell. Microbiol. *19*, e12791. https://doi.org/10.1111/cmi.12791.

15. Tretina, K., Park, E.S., Maminska, A., and MacMicking, J.D. (2019). Interferon-induced guanylate-binding proteins: guardians of host defense in health and disease. J. Exp. Med. *216*, 482–500. https://doi.org/10.1084/jem.20182031.

16. Li, P., Jiang, W., Yu, Q., Liu, W., Zhou, P., Li, J., Xu, J., Xu, B., Wang, F., and Shao, F. (2017). Ubiquitination and degradation of GBPs by a Shigella effector to suppress host defence. Nature *551*, 378–383. https://doi.org/10.1038/nature24467.

17. Zou, Z., Meng, Z., Ma, C., Liang, D., Sun, R., and Lan, K. (2017). Guanylate-binding protein 1 inhibits nuclear delivery of Kaposi's sarcoma-associated herpesvirus virions by disrupting formation of actin filament. J. Virol. *91*, e00632-17. https://doi.org/10.1128/JVI.00632-17.

18. Zhang, J., Zhao, J., Xu, S., Li, J., He, S., Zeng, Y., Xie, L., Xie, N., Liu, T., Lee, K., et al. (2018). Species-specific deamidation of cGAS by herpes simplex virus UL37 protein facilitates viral replication. Cell Host Microbe *24*, 234–248.e5. https://doi.org/10.1016/j.chom.2018.07.004.

19. Sun, X., Liu, T., Zhao, J., Xia, H., Xie, J., Guo, Y., Zhong, L., Li, M., Yang, Q., Peng, C., et al. (2020). DNA-PK deficiency potentiates cGAS-mediated antiviral innate immunity. Nat. Commun. *11*, 6182. https://doi.org/10.1038/s41467-020-19941-0.

20. Zhang, J., He, S., Wang, Y., Brulois, K., Lan, K., Jung, J.U., and Feng, P. (2015). Herpesviral G protein-coupled receptors activate NFAT to induce tumor formation via inhibiting the SERCA calcium ATPase. PLoS Pathog. *11*, e1004768. https://doi.org/10.1371/journal.ppat.1004768.

21. Zhang, J., Feng, H., Zhao, J., Feldman, E.R., Chen, S.Y., Yuan, W., Huang, C., Akbari, O., Tibbetts, S.A., and Feng, P. (2016). IkappaB kinase epsilon is an NFATc1 kinase that inhibits T cell immune response. Cell Rep. *16*, 405–418. https://doi.org/10.1016/j.celrep.2016.05.083.

22. Song, Z.M., Lin, H., Yi, X.M., Guo, W., Hu, M.M., and Shu, H.B. (2020). KAT5 acetylates cGAS to promote innate immune response to DNA virus. Proc. Natl. Acad. Sci. USA *117*, 21568–21575. https://doi.org/10.1073/pnas.1922330117.

23. Zhong, L., Hu, M.M., Bian, L.J., Liu, Y., Chen, Q., and Shu, H.B. (2020). Phosphorylation of cGAS by CDK1 impairs self-DNA sensing in mitosis. Cell Discov. *6*, 26. https://doi.org/10.1038/s41421-020-0162-2.

24. Mukherjee, B., Tomimatsu, N., and Burma, S. (2015). Immunofluorescence-based methods to monitor DNA end resection. Methods Mol. Biol. *1292*, 67–75. https://doi.org/10.1007/978-1-4939-2522-3_5.

25. Praefcke, G.J.K., Kloep, S., Benscheid, U., Lilie, H., Prakash, B., and Herrmann, C. (2004). Identification of residues in the human guanylate-binding protein 1 critical for nucleotide binding and cooperative GTP hydrolysis. J. Mol. Biol. *344*, 257–269. https://doi.org/10.1016/j.jmb.2004.09.026.

26. Piro, A.S., Hernandez, D., Luoma, S., Feeley, E.M., Finethy, R., Yirga, A., Frickel, E.M., Lesser, C.F., and Coers, J. (2017). Detection of cytosolic Shigella flexneri via a C-terminal triple-arginine motif of GBP1 inhibits actin-based motility. mBio *8*, e01979-17. https://doi.org/10.1128/mBio.01979-17.

27. Ostler, N., Britzen-Laurent, N., Liebl, A., Naschberger, E., Lochnit, G., Ostler, M., Forster, F., Kunzelmann, P., Ince, S., Supper, V., et al. (2014). Gamma interferon-induced guanylate binding protein 1 is a novel actin cytoskeleton remodeling factor. Mol. Cell. Biol. *34*, 196–209. https://doi.org/10.1128/MCB.00664-13.

28. Smith, G.A. (2021). Navigating the cytoplasm: delivery of the alphaherpesvirus genome to the nucleus. Curr. Issues Mol. Biol. *41*, 171–220. https://doi.org/10.21775/cimb.041.171.

29. Miranda-Saksena, M., Denes, C.E., Diefenbach, R.J., and Cunningham, A.L. (2018). Infection and transport of herpes simplex virus type 1 in neurons: role of the cytoskeleton. Viruses *10*. https://doi.org/10.3390/v10020092.

30. Wandel, M.P., Pathe, C., Werner, E.I., Ellison, C.J., Boyle, K.B., von der Malsburg, A., Rohde, J., and Randow, F. (2017). GBPs inhibit motility of Shigella flexneri but are targeted for degradation by the bacterial ubiquitin ligase IpaH9.8. Cell Host Microbe *22*, 507–518.e5. https://doi.org/10.1016/j.chom.2017.09.007.

31. Bommareddy, P.K., Peters, C., Saha, D., Rabkin, S.D., and Kaufman, H.L. (2018). Oncolytic herpes simplex viruses as a paradigm for the treatment of cancer. Annu. Rev. Cancer Biol. *2*, 155–173. https://doi.org/10.1146/annurev-cancerbio-030617-050254.

32. Ge, Y., Wang, H., Ren, J., Liu, W., Chen, L., Chen, H., Ye, J., Dai, E., Ma, C., Ju, S., et al. (2020). Oncolytic vaccinia virus delivering tethered IL-12 enhances antitumor effects with improved safety. J. Immunother. Cancer *8*, e000710. https://doi.org/10.1136/jitc-2020-000710.

33. Nakao, S., Arai, Y., Tasaki, M., Yamashita, M., Murakami, R., Kawase, T., Amino, N., Nakatake, M., Kurosaki, H., Mori, M., et al. (2020). Intratumoral expression of IL-7 and IL-12 using an oncolytic virus increases systemic sensitivity to immune checkpoint blockade. Sci. Transl. Med. *12*, eaax7992. https://doi.org/10.1126/scitranslmed.aax7992.

34. Choi, I.K., Lee, J.S., Zhang, S.N., Park, J., Sonn, C.H., Lee, K.M., and Yun, C.O. (2011). Oncolytic adenovirus co-expressing IL-12 and IL-18 improves tumor-specific immunity via differentiation of T cells expressing IL-12R beta(2) or IL-18R alpha (vol 18, pg 898, 2011). Gene Ther. *18*, 942. https://doi.org/10.1038/gt.2011.72.

35. Parker, J.N., Gillespie, G.Y., Love, C.E., Randall, S., Whitley, R.J., and Markert, J.M. (2000). Engineered herpes simplex virus expressing IL-12 in the treatment of experimental murine brain tumors. Proc. Natl. Acad. Sci. USA *97*, 2208–2213. https://doi.org/10.1073/pnas.040557897.

36. Rosewell Shaw, A., Porter, C.E., Watanabe, N., Tanoue, K., Sikora, A., Gottschalk, S., Brenner, M.K., and Suzuki, M. (2017). Adenovirotherapy delivering cytokine and checkpoint inhibitor augments CAR T cells against metastatic head and neck cancer. Mol. Ther. *25*, 2440–2451. https://doi.org/10.1016/j.ymthe.2017.09.010.

37. Kleinpeter, P., Fend, L., Thioudellet, C., Geist, M., Sfrontato, N., Koerper, V., Fahrner, C., Schmitt, D., Gantzer, M., Remy-Ziller, C., et al. (2016). Vectorization in an oncolytic vaccinia virus of an antibody, a Fab and a scFv against programmed cell death-1 (PD-1) allows their intratumoral delivery and an improved tumor-growth inhibition. Oncoimmunology *5*, e1220467. https://doi.org/10.1080/2162402X.2016.1220467.

38. Wang, G., Kang, X., Chen, K.S., Jehng, T., Jones, L., Chen, J., Huang, X.F., and Chen, S.Y. (2020). An engineered oncolytic virus expressing PD-L1 inhibitors activates tumor neoantigen-specific T cell responses. Nat. Commun. *11*, 1395. https://doi.org/10.1038/s41467-020-15229-5.

39. Wilcox, D.R., and Longnecker, R. (2016). The herpes simplex virus neurovirulence factor gamma 34.5: revealing virus-host interactions. PLoS Pathog. *12*, e1005449. https://doi.org/10.1371/journal.ppat.1005449.

40. Manivanh, R., Mehrbach, J., Knipe, D.M., and Leib, D.A. (2017). Role of herpes simplex virus 1 gamma34.5 in the regulation of IRF3 signaling. J. Virol. *91*, e01156-17. https://doi.org/10.1128/JVI.01156-17.

41. Yoo, J.Y., Hurwitz, B.S., Bolyard, C., Yu, J.G., Zhang, J., Selvendiran, K., Rath, K.S., He, S., Bailey, Z., Eaves, D., et al. (2014). Bortezomib-induced unfolded protein response increases oncolytic HSV-1 replication resulting in synergistic antitumor effects. Clin. Cancer Res. *20*, 3787–3798. https://doi.org/10.1158/1078-0432.CCR-14-0553.

42. Nakashima, H., Kaufmann, J.K., Wang, P.Y., Nguyen, T., Speranza, M.C., Kasai, K., Okemoto, K., Otsuki, A., Nakano, I., Fernandez, S., et al. (2015). Histone deacetylase 6 inhibition enhances oncolytic viral replication in glioma. J. Clin. Invest. *125*, 4269–4280. https://doi.org/10.1172/JCI80713.

43. Passer, B.J., Cheema, T., Zhou, B., Wakimoto, H., Zaupa, C., Razmjoo, M., Sarte, J., Wu, S., Wu, C.L., Noah, J.W., et al. (2010). Identification of the ENT1 antagonists dipyridamole and dilazep as amplifiers of oncolytic herpes simplex virus-1 replication. Cancer Res. *70*, 3890–3895. https://doi.org/10.1158/0008-5472.CAN-10-0155.

44. Crameri, M., Bauer, M., Caduff, N., Walker, R., Steiner, F., Franzoso, F.D., Gujer, C., Boucke, K., Kucera, T., Zbinden, A., et al. (2018). MxB is an interferon-induced restriction factor of human herpesviruses. Nat. Commun. *9*, 1980. https://doi.org/10.1038/s41467-018-04379-2.

45. Tanaka, M., Kagawa, H., Yamanashi, Y., Sata, T., and Kawaguchi, Y. (2003). Construction of an excisable bacterial artificial chromosome containing a full-length infectious clone of herpes simplex virus type 1: viruses reconstituted from the clone exhibit wild-type properties in vitro and in vivo. J. Virol. *77*, 1382–1391. https://doi.org/10.1128/jvi.77.2.1382-1391.2003.

46. Richards, A.L., Sollars, P.J., and Smith, G.A. (2016). New tools to convert bacterial artificial chromosomes to a self-excising design and their application to a herpes simplex virus type 1 infectious clone. BMC Biotechnol. *16*, 64. https://doi.org/10.1186/s12896-016-0295-4.

47. Wang, I.H., Suomalainen, M., Andriasyan, V., Kilcher, S., Mercer, J., Neef, A., Luedtke, N.W., and Greber, U.F. (2013). Tracking viral genomes in host cells at single-molecule resolution. Cell Host Microbe *14*, 468–480. https://doi.org/10.1016/j.chom.2013.09.004.